


RESEARCH

Open Access



Early detection of amyloid load using ^{18}F -florbetaben PET

Santiago Bullich^{1*†} , Núria Roé-Vellvé^{1†}, Marta Marquíe^{2,3}, Susan M. Landau⁴, Henryk Barthel⁵, Victor L. Villemagne^{6,7}, Ángela Sanabria^{2,3}, Juan Pablo Tartari², Oscar Sotolongo-Grau², Vincent Doré^{7,8}, Norman Koglin¹, Andre Müller¹, Audrey Perrotin¹, Aleksandar Jovalekic¹, Susan De Santi⁹, Lluís Tárraga^{2,3}, Andrew W. Stephens¹, Christopher C. Rowe⁷, Osama Sabri⁵, John P. Seibyl¹⁰ and Mercè Boada^{2,3}

Abstract

Background: A low amount and extent of A β deposition at early stages of Alzheimer's disease (AD) may limit the use of previously developed pathology-proven composite SUVR cutoffs. This study aims to characterize the population with earliest abnormal A β accumulation using ^{18}F -florbetaben PET. Quantitative thresholds for the early (SUVR_{early}) and established (SUVR_{estab}) A β deposition were developed, and the topography of early A β deposition was assessed. Subsequently, A β accumulation over time, progression from mild cognitive impairment (MCI) to AD dementia, and tau deposition were assessed in subjects with early and established A β deposition.

Methods: The study population consisted of 686 subjects ($n = 287$ (cognitively normal healthy controls), $n = 166$ (subjects with subjective cognitive decline (SCD)), $n = 129$ (subjects with MCI), and $n = 101$ (subjects with AD dementia)). Three categories in the A β -deposition continuum were defined based on the developed SUVR cutoffs: A β -negative subjects, subjects with early A β deposition ("gray zone"), and subjects with established A β pathology.

Results: SUVR using the whole cerebellum as the reference region and centiloid (CL) cutoffs for early and established amyloid pathology were 1.10 (13.5 CL) and 1.24 (35.7 CL), respectively. Cingulate cortices and precuneus, frontal, and inferior lateral temporal cortices were the regions showing the initial pathological tracer retention. Subjects in the "gray zone" or with established A β pathology accumulated more amyloid over time than A β -negative subjects. After a 4-year clinical follow-up, none of the A β -negative or the gray zone subjects progressed to AD dementia while 91% of the MCI subjects with established A β pathology progressed. Tau deposition was infrequent in those subjects without established A β pathology.

(Continued on next page)

* Correspondence: sbullich@life-mi.com

†Santiago Bullich and Núria Roé-Vellvé contributed equally to this work.

¹Life Molecular Imaging GmbH, Tegeler Str. 6-7, 13353 Berlin, Germany

Full list of author information is available at the end of the article



© The Author(s). 2021 **Open Access** This article is licensed under a Creative Commons Attribution 4.0 International License, which permits use, sharing, adaptation, distribution and reproduction in any medium or format, as long as you give appropriate credit to the original author(s) and the source, provide a link to the Creative Commons licence, and indicate if changes were made. The images or other third party material in this article are included in the article's Creative Commons licence, unless indicated otherwise in a credit line to the material. If material is not included in the article's Creative Commons licence and your intended use is not permitted by statutory regulation or exceeds the permitted use, you will need to obtain permission directly from the copyright holder. To view a copy of this licence, visit <http://creativecommons.org/licenses/by/4.0/>. The Creative Commons Public Domain Dedication waiver (<http://creativecommons.org/publicdomain/zero/1.0/>) applies to the data made available in this article, unless otherwise stated in a credit line to the data.

(Continued from previous page)

Conclusions: This study supports the utility of using two cutoffs for amyloid PET abnormality defining a “gray zone”: a lower cutoff of 13.5 CL indicating emerging A β pathology and a higher cutoff of 35.7 CL where amyloid burden levels correspond to established neuropathology findings. These cutoffs define a subset of subjects characterized by pre-AD dementia levels of amyloid burden that precede other biomarkers such as tau deposition or clinical symptoms and accelerated amyloid accumulation. The determination of different amyloid loads, particularly low amyloid levels, is useful in determining who will eventually progress to dementia. Quantitation of amyloid provides a sensitive measure in these low-load cases and may help to identify a group of subjects most likely to benefit from intervention.

Trial registration: Data used in this manuscript belong to clinical trials registered in ClinicalTrials.gov ([NCT00928304](#), [NCT00750282](#), [NCT01138111](#), [NCT02854033](#)) and EudraCT (2014-000798-38).

Keywords: Florbetaben, PET, Amyloid-beta, Subjective memory complainers, Mild cognitive impairment, Alzheimer's disease

Background

Extracellular amyloid-beta (A β) aggregates are a key pathologic hallmark of Alzheimer's disease (AD) [1]. Aggregation of A β is a slow and protracted process which may extend for more than two decades before the onset of clinical symptoms [2]. The lack of success of anti-A β therapeutic clinical trials in reducing the cognitive decline in AD [3, 4] has encouraged investigators to start intervention at the earliest possible phase when abnormalities in amyloid biomarkers are detectable even at the asymptomatic stage [5–8].

Amyloid positron emission tomography (PET) with ¹⁸F-florbetaben is an established biomarker of A β deposition [9]. Visual assessment of ¹⁸F-florbetaben PET is used in the clinical setting to estimate A β neuritic plaque density and to classify scans as A β -positive or A β -negative. Visual assessment was validated against histopathological confirmation of the presence of A β deposition [9, 10], but it is dichotomous and may lack sensitivity to assess longitudinal changes. In the research setting, a quantitative approach using composite standardized uptake value ratios (SUVRs) calculated from selected cerebral cortical areas is currently being used as a screening tool in clinical trials and is able to detect A β changes either in clinical trials after an anti-A β drug is administered or in longitudinal observational studies [11]. ¹⁸F-Florbetaben PET SUVR abnormality cutoffs have also been developed to accurately categorize scans [12]. An SUVR abnormality cutoff of 1.478 in a global cortical composite region relative to the cerebellar cortex was developed using histopathological confirmation as the standard of truth providing excellent sensitivity (89.4%) and specificity (92.3%) to detect established A β pathology [9]. Other groups have developed other SUVR abnormality cutoffs for ¹⁸F-florbetaben PET ranging from 1.38 to 1.45 using different populations, analytical methods, and standards of truth [10, 12–18]. These SUVR cutoffs, however, were developed with the aim of

discriminating between subjects with established A β pathology (e.g., AD) and other populations (e.g., cognitively normal elderly subjects). Therefore, these global SUVR cutoffs are not optimal to detect the earliest abnormal pathophysiological accumulation of amyloid load and do not provide topographical information. In addition, several studies have shown that measures of A β deposition below a threshold of established A β pathology carry critical information on initial pathological brain changes and may indicate appropriate time periods for interventions [19]. Moreover, the regional evolution of A β load may enable earlier identification of subjects in the AD pathologic continuum and may overcome dichotomous measures [20]. Regional information has shown to be relevant in staging A β pathology [21–23], tracking disease progression, and assessing the risk of cognitive decline [23–25].

The aim of this study was to characterize the population with the earliest abnormal pathophysiological A β accumulation using ¹⁸F-florbetaben PET and to identify those subjects that will likely accumulate A β over time. To this end, a sample of young cognitively normal subjects (20–40 years) scanned with ¹⁸F-florbetaben PET was used to develop regional SUVR cutoffs to detect early A β accumulation. Subsequently, the topography of abnormal A β accumulation, A β accumulation over time, progression to AD dementia, and tau deposition were assessed in older cognitively impaired or cognitively unimpaired individuals with early and established A β accumulation.

Materials and methods

Participants

The study population consisted of 686 subjects who underwent at least one ¹⁸F-florbetaben PET and T1-weighted MRI scans in established research cohort studies summarized in Table 1. The clinical diagnosis of the study participants included young and cognitively

Table 1 Summary of the participants in the study

Dataset identifier	Source	Clinical diagnosis	Number	Age	M/F	Methods
#1	NCT00928304 [†]	yHC	65	27.4 ± 5.1	25/40	Sample of yHC (20–40 yrs) that underwent a ¹⁸ F-florbetaben PET scan. This subset was used to develop an SUVR cutoff for early A β accumulation.
#2	NCT00750282 [13]	eHC AD	66 73	68.0 ± 6.9 71.0 ± 7.9	28/38 41/32	All subjects underwent a ¹⁸ F-florbetaben PET scan. This subset was used to develop an SUVR cutoff for established A β pathology using ROC analysis.
#3	EudraCT: 2014-000798-38 [26]	SCD	168	64.9 ± 7.3	65/103	SCD patients from the Fundació ACE Healthy Brain Initiative (FACEHBI) study that underwent two ¹⁸ F-florbetaben PET scans at baseline and after 2 years. This subset was used to assess the A β accumulation over time.
#4	NCT01138111 [18]	MCI	44	72.6 ± 6.6	28/16	MCI subjects that underwent three ¹⁸ F-florbetaben PET scans at baseline ($n = 44$), 1 yr ($n = 40$), and 2 yrs ($n = 35$) and a 4-year clinical follow-up. This subset was used to assess the A β accumulation over time and conversion to AD.
#5	NCT02854033 (ADNI3 [‡])	eHC MCI AD	157 85 28	70.6 ± 6.1 71.7 ± 8.1 71.3 ± 7.0	62/95 47/38 18/10	Subjects from the ADNI3 study that underwent a ¹⁸ F-florbetaben PET and a ¹⁸ F-flortaucipir PET. This subset was used to assess the association between A β and tau deposition.

[†]Unpublished methods on the sample of yHC are provided in the supplemental material 1

[‡]Part of the data used in the preparation of this article were obtained from the Alzheimer's Disease Neuroimaging Initiative (ADNI) database (adni.loni.usc.edu). The ADNI was launched in 2003 as a public-private partnership, led by Principal Investigator Michael W. Weiner, MD. The primary goal of ADNI has been to test whether serial magnetic resonance imaging, positron emission tomography, other biological markers, and clinical and neuropsychological assessment can be combined to measure the progression of mild cognitive impairment and early Alzheimer's disease. For up-to-date information, see www.adni-info.org
 Abbreviations: yHC young healthy controls, eHC elderly healthy controls, AD Alzheimer's disease dementia, SCD subjective cognitive decline, MCI mild cognitive impairment, SUVR standardized uptake value ratio, PET positron emission tomography, M male, F female, A β amyloid-beta, ROC receiver operating characteristic

normal healthy controls (20–40 years) (yHC, $n = 65$), elderly healthy controls (eHC, $n = 223$), subjects with subjective cognitive decline (SCD, $n = 168$), subjects with mild cognitive impairment (MCI, $n = 129$), and subjects with AD dementia ($n = 101$). The sample of yHC ($n = 65$) (dataset #1) was used to develop an SUVR cutoff for early A β accumulation. A sample of eHC ($n = 66$) and AD ($n = 73$) subjects (dataset #2) was used to develop an SUVR cutoff for established A β pathology using ROC analysis. A subset of participants with SCD and MCI ($n = 212$) (datasets #3 and #4) underwent two or three ¹⁸F-florbetaben PET scans to assess A β deposition over time. A subset of MCI subjects (datasets #4) that underwent three ¹⁸F-florbetaben PET scans at baseline ($n = 44$), 1 year ($n = 40$), and 2 years ($n = 35$) and a 4-year clinical follow-up was used to assess conversion to AD dementia in addition to A β deposition over time. Another subset of participants (dataset #5) ($n = 157$ (eHC), $n = 85$ (MCI), $n = 28$ (AD)) underwent a ¹⁸F-flortaucipir PET in addition to the ¹⁸F-florbetaben PET to assess the association between A β and tau deposition. Subjects from the ADNI study were not assessed visually. The demographic characteristics of the samples and image acquisition methods are summarized in Table 1 and supplemental material 1.

Image analysis

¹⁸F-Florbetaben acquisition and image processing

Details on the PET image acquisition and reconstruction are provided in the respective original

publication of the studies used (Table 1). In short, all subjects underwent a 20-min PET scan (4 × 5 min dynamic frames) starting at least 90 min after intravenous injection of 300 MBq ± 20% of ¹⁸F-florbetaben followed by a 10-mL saline flush. PET scans were reconstructed using Ordered Subsets Expectation Maximization (OSEM) algorithm using 4 iterations and 16 subsets (zoom = 2) or comparable reconstruction. Corrections were applied for attenuation, scatter, randoms, and dead time. Three-dimensional volumetric T1-weighted brain magnetic resonance imaging (MRI) data was also collected. Then, a Gaussian smoothing kernel was applied to all the scans to bring the ¹⁸F-florbetaben PET images from different scanner models to a uniform 8 × 8 × 8 mm spatial resolution. The Gaussian smoothing kernel for each scanner was determined using previously acquired Hoffman brain phantoms [27]. Image analysis of ¹⁸F-florbetaben PET scans was conducted using SPM8 (<https://www.fil.ion.ucl.ac.uk/spm/software/spm8/>). Motion correction was performed on each PET frame, and an average PET image was generated. Then, the average PET scan was co-registered to its associated T1-weighted MRI scan. Subsequently, the MRI image was segmented into gray matter, white matter, and cerebrospinal fluid, and spatially normalized to the standard MNI (Montreal Neurological Institute) space. The normalization transformation was applied to the co-registered PET scans and gray matter probability maps.

MRI-derived ROIs Regions of interest (ROIs) were defined as the intersection between the standard Automated Anatomic Labeling (AAL) atlas [28] and the normalized gray matter segmentation map thresholded at a probability level of 0.2. ROIs included the cerebellar gray matter and frontal (orbitofrontal and prefrontal), lateral temporal (inferior and superior), occipital, parietal, precuneus, anterior cingulate, posterior cingulate, striatum, amygdala, and thalamus. Mean radioactivity values were obtained from each ROI without correction for partial volume effects applied to the PET data. SUVR was calculated as the ratio of the activity in the target ROI to the activity in the reference region ROI (cerebellar gray matter). A composite SUVR was calculated by unweighted averaging the SUVR of the 6 cortical regions (frontal, lateral temporal, occipital, parietal, anterior, and posterior cingulate cortices) [29].

Calibration to centiloid (CL) scale Given that SUVR values may depend on the tracer used and analytical methods, all the analysis of this paper were provided in CL scale to make the cutoffs useful to other groups or when using other amyloid tracers. Centiloid (CL) values were calculated for each ^{18}F -florbetaben PET using the method described by Klunk et al. [30]. ROIs downloaded from the Global Alzheimer's Association Interactive Network (GAAIN) website (<http://www.gaain.org>) for the cerebral cortex and the whole cerebellum were applied to the normalized ^{18}F -florbetaben PET. Cortical SUVR was calculated as the ratio of the activity in the cortex to the activity in the reference region ROI (whole cerebellum). Finally, the CL values were calculated ($\text{CL} = 153.4 \cdot \text{SUVR} - 154.9$) [31]. The in-house implementation of the standard CL analysis was validated using data freely accessible at the GAAIN website (<http://www.gaain.org>). SUVRs and CL values from the validation dataset were compared by means of linear correlation to those reported by Klunk et al. [30] ($\text{SUVR}_{\text{Klunk}}, \text{CL}_{\text{Klunk}}$). The in-house implementation of standard CL analysis passed all the validation criteria described by Klunk et al. [30] being $\text{SUVR} = 1.01 \text{ SUVR}_{\text{Klunk}} - 0.01$ ($R^2 = 0.998$) and $\text{CL} = 1.00 \text{ CL}_{\text{Klunk}} + 0.00$ ($R^2 = 1.00$) the regression lines when the whole cerebellum was used as the reference region.

^{18}F -Flortaucipir (^{18}F -AV1451) acquisition and image processing

Details on the PET image acquisition and reconstruction are provided in ADNI3 PET technical procedures manual (https://adni.loni.usc.edu/wp-content/uploads/2012/10/ADNI3_PET-Tech-Manual_V2.0_20161206.pdf). In short, all subjects underwent a 30-min PET scan (6×5 min dynamic frames) starting at 75 min after intravenous injection of $370 \text{ MBq} \pm 10\%$ of flortaucipir. Image

analysis of ^{18}F -flortaucipir PET scans was performed using the same methods described for ^{18}F -florbetaben PET analysis. Cortical ROIs extracted from the AAL atlas included the mesial temporal (average of amygdala, hippocampus, and parahippocampus), fusiform gyrus, inferior lateral temporal, parietal cortices, and cerebellar gray matter. SUVR was calculated as the ratio of the activity in the cortical ROIs to the activity in the reference region (cerebellar gray matter excluding vermis and anterior lobe cerebellar surrounding the vermis).

Visual assessment

Amyloid PET scans from a subset of 416 participants ($n = 65$ (yHC), $n = 66$ (eHC), $n = 168$ (SCD), $n = 44$ (MCI), $n = 73$ (AD)) (datasets #1, #2, #3, and #4) were visually assessed by independent blinded readers using the method described in Seibyl et al. [10]. The readers were blinded to any structural information (CT or MRI) and different for each of the studies included in the manuscript. The subjects used to generate cutoffs for the detection of established A β amyloid pathology (dataset #2) and MCI subjects (dataset #4) were read by 3 independent blinded readers with previous experience reading FBB scans and the final assessment was based on the majority read (i.e., agreement of the majority of readers).

SUVR cutoff development and definition of the gray zone *Development of an SUVR cutoff for the detection of early A β deposition (SUVR_{early})*

A group of visually A β -negative cognitively normal yHC (dataset #1) were used to develop an SUVR cutoff to detect early amyloid deposition. A Shapiro-Wilk test was applied to ascertain that the distribution of each regional SUVR was not significantly different from the Gaussian distribution. Then, the regional SUVR_{early} cutoffs were calculated as 2 standard deviations above the mean SUVR of the yHC.

Development of an SUVR cutoff for the detection of established A β pathology (SUVR_{estab})

The established pathology SUVR cutoff was derived using receiver operating characteristic (ROC) analysis to ascertain the optimal threshold for the sensitivity and specificity calculation on a sample of visually A β -negative eHC and visually A β -positive AD dementia patients (dataset #2) [13]. The SUVR that provided the highest Youden's index (sensitivity + specificity - 1) was selected. In cases that several SUVR provided the same Youden's index, the SUVR with higher specificity was selected. Global visual assessment as described by Seibyl et al. was used as the standard of truth [10].

Definition of the “gray zone”

Given the developed SUVR cutoffs, three groups were defined within the SUVR continuum: Aβ-negative subjects ($SUVR < SUVR_{early}$), early Aβ deposition or “gray zone” ($SUVR_{early} \leq SUVR \leq SUVR_{estab}$), and Aβ-positive subjects with established amyloid pathology ($SUVR_{estab} < SUVR$).

Characterization of earliest in vivo signal and SUVR cutoff assessment

Characterization of earliest in vivo signal in amyloid PET images and topographical distribution

Given that each brain region may have different non-specific binding and dynamic SUVR ranges, direct comparison of SUVR across regions cannot be used to extract the regions showing the earliest amyloid deposition. The assessment of early amyloid deposition assumed that amyloid accumulation follows a logistic growth [32]:

$$SUVR(t) = NS + \frac{K}{1 + e^{-r(t - T_{50})}}$$

where t is the time through the accumulation process, $SUVR(t)$ is the regional SUVR at time t , NS is the tracer non-specific binding, r is the exponential uninhibited growth rate, K is the carrying capacity, and T_{50} is the time of half-maximal Aβ carrying capacity. NS, K , r , and T_{50} could be different for each region. However, the logistic growth model could not be fitted given the cross-sectional nature of the data used in this work (i.e., individual times through the accumulation process are unknown). Instead, half of the maximum amyloid carrying capacity ($SUVR(t = T_{50})$) reached when $t = T_{50}$ was used to identify those regions that show earliest amyloid signal using PET. In this study, it was hypothesized that T_{50} will be smallest in regions with early amyloid deposition.

$$SUVR(t = T_{50}) = NS + \frac{K}{2}$$

where NS was estimated from the regional mean SUVR of the visually Aβ-negative yHCs ($NS = SUVR_{yHC}$) and K was estimated from the difference between the regional mean of visually Aβ-positive AD dementia subjects ($SUVR_{AD}$) and $SUVR_{yHC}$ ($K = SUVR_{AD} - SUVR_{yHC}$).

$$SUVR(t = T_{50}) = \frac{SUVR_{AD} + SUVR_{yHC}}{2}$$

Then, a regional $\Delta SUVR$ was derived to characterize the location of a subject in the AD continuum as follows: $\Delta SUVR = SUVR - SUVR(t = T_{50})$. The $\Delta SUVR$ takes positive values in those subjects and regions that are above $SUVR(t = T_{50})$ and close to the SUVR of

subjects with AD dementia and negative values in those subjects and regions that are close to SUVR of yHC. $\Delta SUVR$ score was compared across regions. Those regions that reached half of the maximum amyloid carrying capacity ($\Delta SUVR = 0$) earlier were considered the regions that show earliest amyloid deposition. Amygdala, thalamus, and striatum, which have a limited dynamic SUVR range between yHC and subjects with AD dementia due to low tracer accumulation, were not included in the interpretation of $\Delta SUVR$ s.

Assessment of Aβ accumulation

In this study, it was hypothesized that subjects with SUVR in the “gray zone” are in the initial stages of Aβ accumulation. To test this hypothesis, Aβ accumulation was assessed in two samples of SCD and MCI subjects with longitudinal ¹⁸F-florbetaben PET scans (datasets #3 and #4). To estimate the annual SUVR increase, a linear regression model was fitted to each subject’s data, $SUVR = \alpha \cdot t + \beta$, where α and β are the coefficients of the model, and t is the scan time in years. The annual SUVR increase was obtained from α . The percent of Aβ deposition per year ($A\beta_{dep}$) was determined as $A\beta_{dep} = 100 \cdot \alpha / SUVR_B$ where $SUVR_B$ is the SUVR at baseline. Subsequently, the average annual SUVR increase (α) in each sample was tested statistically by means of a t -test to demonstrate that those subjects in the “gray zone” are in the process of accumulating Aβ (i.e., ($H_0 : \alpha = 0$; $H_1 : \alpha > 0$)). Likewise, annual CL increase (α_{CL}) was estimated using a linear regression model fitted to each subject’s data, $CL = \alpha_{CL} t + \beta_{CL}$, where α_{CL} and β_{CL} are the coefficients of the model and t is the scan time in years.

Assessment of tau deposition

In subjects that underwent a tau PET scan (dataset #5), ¹⁸F-flortaucipir SUVR (mean ± SD) was estimated in the three cutoff-based groups (Aβ-negative subjects, subjects in the “gray zone”, and Aβ-positive subjects with established amyloid pathology) and compared by means of a t -test.

Sensitivity of visual assessment to detect early amyloid accumulation

In those subjects assessed visually (datasets #1, #2, #3, and #4), the proportion of visually Aβ-positive scans was estimated in the three cutoff-based groups (Aβ-negative subjects, subjects in the “gray zone”, and Aβ-positive subjects with established amyloid pathology) to assess the sensitivity of visual assessment to detect early amyloid accumulation.

Results

Development of SUVR_{early} cutoff

A sample of cognitively normal yHC was used to develop the SUVR cutoff to detect early amyloid deposition. The distribution of SUVRs in yHC did not statistically differ from a Gaussian distribution being the Shapiro-Wilk test non-significant ($p > 0.05$) in any of the regions analyzed (Fig. 1, Table 2). The composite SUVR using MRI-derived ROIs in the yHC was 1.16 ± 0.04 (mean \pm SD) resulting in a SUVR_{early} cutoff of 1.25 (Fig. 1, Table 2). The determined SUVR_{early} cutoff differed across regions ranging from 1.15 (lateral temporal cortex) and 1.45 (posterior cingulate cortex) (Table 2). When the standard CL ROIs were applied, the mean of the yHC was 1.03 ± 0.03 (2.82 ± 5.36 CL) and the resulting cutoff (CL_{early}) was 1.10 (13.5 CL) (Table 2).

Development of the SUVR_{estab} cutoff

ROC analysis using visual assessment as the standard of truth resulted in SUVR_{estab} cutoffs ranging from 1.26 (lateral temporal and parietal cortices) to 1.47 (posterior cingulate cortex). The SUVR cutoff (MRI-derived ROIs) for the composite region was 1.38 (Fig. 2, Table 3). When the standard CL analysis was applied, the SUVR_{estab} and CL_{estab} cutoff obtained were 1.24 and 35.7 CL, respectively.

Earliest in vivo signal in amyloid PET images and topographical distribution

Posterior and anterior cingulate cortices followed by precuneus, frontal, and inferior temporal cortices were the regions that showed earlier elevated SUVR values (Fig. 3, left panel). However, given that each region has a different non-specific uptake and SUVR dynamic range, the regional SUVRs were compared against the half maximum amyloid carrying capacity

by means of Δ SUVR (Δ SUVR = SUVR - SUVR($t = T_{50}$)) to determine the regions that show earliest amyloid accumulation (Fig. 3, right panel). Cingulate cortices (anterior and posterior), precuneus, and orbitofrontal were the regions that first showed pathological A β PET tracer retention followed by prefrontal, inferior lateral temporal, parietal, and occipital cortices (Fig. 3, right panel). Other regions that showed tracer retention and differences from yHC were the striatum and the amygdala.

A β deposition in subjects with SCD

SUVR histograms derived from a sample of subjects with SCD showed a peak coincident with the Gaussian function fitted to the sample of yHC with a tail with higher SUVRs that increased numbers at follow-up (Fig. 4). The rate of amyloid accumulation increased significantly in those subjects with SUVR in the “gray zone” or with established A β deposition in comparison with A β -negative subjects ($p < 0.002$) (Fig. 4). The subjects with SUVRs in the “gray zone” and established A β deposition had rates of A β accumulation statically different from zero ($p < 0.001$) ($1.66 \pm 1.86\%/year$ (composite) and $2.40 \pm 2.37\%/year$ (composite), respectively) (Fig. 4, Table 4). Similar results were obtained when the CL analysis was used (1.81 ± 1.86 CL/year ($p < 0.001$)) (gray zone), 2.38 ± 1.82 CL/year ($p < 0.001$) (established A β pathology)). In general, the A β accumulation was significantly larger for subjects in the gray zone and established A β deposition than in A β -negative subjects (Fig. 4, Table 4).

Progression to AD dementia in MCI subjects

SUVR histograms obtained from the MCI subjects showed a broad range of SUVRs (Fig. 5). In general, the rate of amyloid accumulation increased significantly in those subjects with SUVR in the “gray zone” or with established A β deposition in comparison with A β -negative subjects ($p < 0.05$). However, the difference between A β -negative subjects and subjects in the “gray zone” did not reach statistical significance when CL ROIs were used (Fig. 5). In the composite region, the rate of A β accumulation in the “gray zone” ($1.51 \pm 1.38\%/year$ ($p = 0.04$)) and for “established A β deposition” ($1.23 \pm 1.90\%/year$ ($p = 0.004$)) was significantly different from zero (Fig. 5) while no accumulation was found in A β -negative subjects ($-0.29 \pm 1.68\%/year$ ($p = 0.74$)) (Table 5). None of the A β -negative subjects or subjects in the “gray zone” progressed to AD dementia after a 4-year clinical follow-up. Twenty-one subjects (91%) with SUVR above SUVR_{estab} progressed to AD dementia after 4 years (Fig. 5).

Table 2 SUVRs of yHC (dataset #1, $n = 65$) and cutoffs for the detection of early A β accumulation (between parenthesis)

Method	Region	SUVR _{yHC} (cutoff)	<i>p</i>
MRI-derived ROIs	Frontal	1.09 ± 0.04 (1.16)	0.83
	Lateral temporal	1.09 ± 0.03 (1.15)	0.41
	Occipital	1.18 ± 0.04 (1.26)	0.93
	Parietal	1.12 ± 0.04 (1.20)	0.92
	Anterior cingulate	1.23 ± 0.07 (1.36)	0.13
	Posterior cingulate	1.28 ± 0.09 (1.45)	0.43
	Precuneus	1.12 ± 0.04 (1.21)	0.22
	Composite	1.16 ± 0.04 (1.25)	0.25
CL ROIs	Cortex	1.03 ± 0.03 (1.10)	0.32
		2.82 ± 5.36 CL (13.54 CL)	

yHC young healthy controls, SUVR_{yHC} SUVR (mean \pm SD) of the young healthy controls, A β amyloid-beta, *p* *p*-values from the Shapiro-Wilk test to assess that SUVR values are normally distributed ($p < 0.05$ = significant differences from the normality)

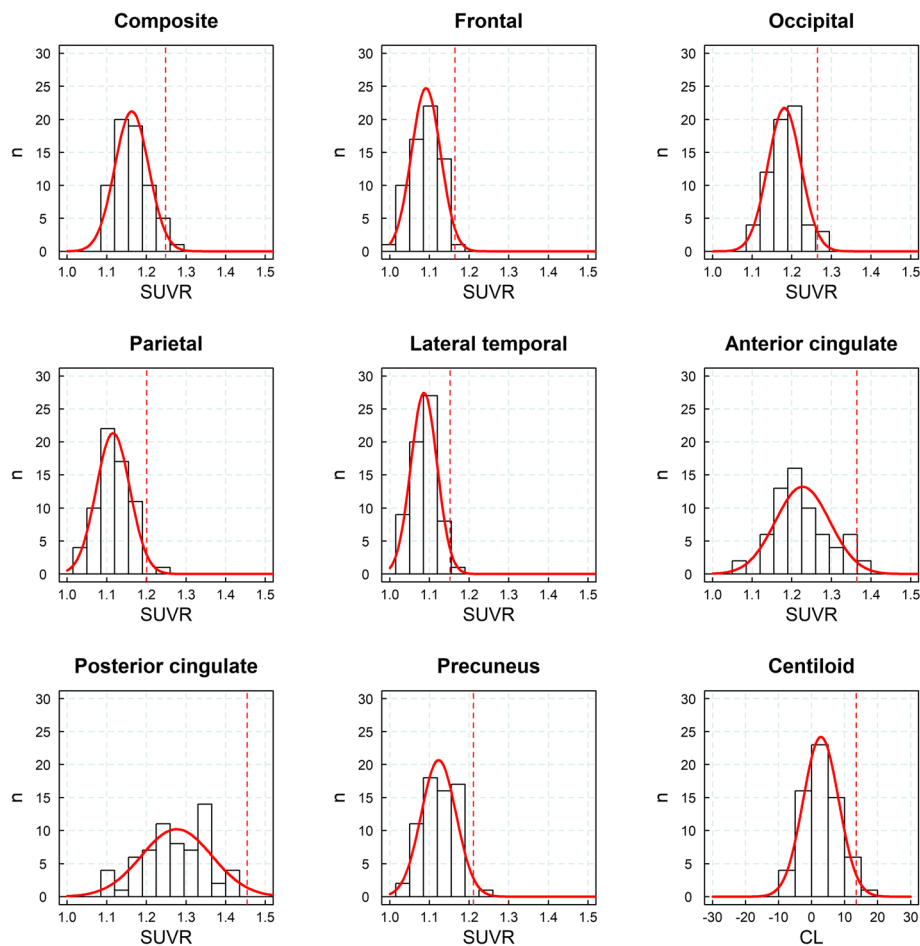


Fig. 1 Histograms of standardized uptake value ratios (SUVRs) and cortex centiloids (CLs) in young healthy controls ($n = 65$, dataset #1), fitted Gaussian distribution (red), and SUVR cutoff derived for the detection of early A β pathology (red dashed line)

Association between A β load and tau deposition

Figure 6 shows the association between amyloid load measured with ^{18}F -florbetaben and tau load measured with [^{18}F] flortaucipir ($\rho = 0.35$ (parietal)– 0.54 (fusiform gyrus) (ρ : Spearman correlation coefficient); $p < 0.0001$) (Table 6, Fig. 6). Tau deposition was rarely observed in A β -negative subjects and subjects in the gray zone: ($\text{SUVR}^{(18\text{F-flortaucipir})} = 1.15 \pm 0.08$ (A β -negative), 1.16 ± 0.09 (gray zone) (Fusiform gyrus)), but increased in subjects with established A β pathology ($\text{SUVR}^{(18\text{F-flortaucipir})} = 1.35 \pm 0.24$ (Fusiform gyrus)) (Table 6).

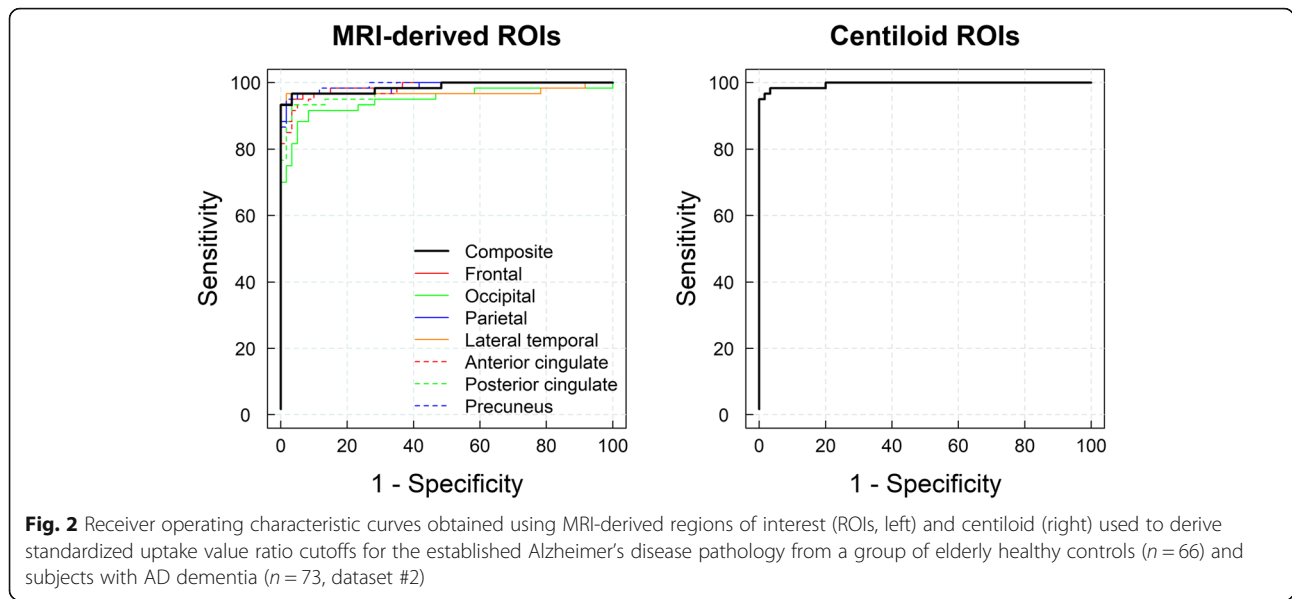
Sensitivity of visual assessment to detect early amyloid accumulation

Most of the subjects with established A β pathology defined either by SUVR (MRI-derived ROIs) or CL cutoffs were visually assessed as positive (93% and 95%, respectively), while all the subjects in the A β -negative group were visually assessed as negative (100%). In the gray zone, only 21.4% (MRI-derived ROIs) and 19.6% (CL) of the subjects were visually assessed as positive. The

maximum agreement between visual assessment and quantitative assessment was found for SUVR and CL cutoffs in the upper range of the gray zone, while the agreement decreased in the lower range of the gray zone (Fig. 7).

Discussion

Currently, observational and interventional studies focus on earlier stages of A β deposition, where established SUVR cutoffs to discriminate AD dementia subjects from elderly HC are of limited value. In this study, regional and global quantitative SUVR cutoffs were developed for the detection of early amyloid accumulation and established A β pathology using ^{18}F -florbetaben PET. A gray zone was defined as the range of SUVR values in subjects having higher SUVR than yHC and less than the values previously used to define visual positivity in patients with AD dementia. The existence of a “gray zone” that may precede visual positivity and the feasibility of identifying subjects in the gray zone using ^{18}F -florbetaben PET were corroborated using two quantitative



methods (MRI-derived ROIs and CL ROIs). The population in the “gray zone” represents early stages of A β deposition characterized by accelerated A β accumulation and pre-AD dementia levels of A β burden that may precede the alteration of other biomarkers such as tau deposition or clinical symptoms. Although assessment of tau deposition using Flortaucipir PET in mesial temporal structures could be biased due to adjacent choroid plexus uptake, the association between A β and tau was strong also in other regions assessed such as fusiform gyrus and inferior lateral temporal cortex. While the agreement between visual and quantitative assessments was excellent for A β -negative subjects and subjects with established A β pathology, the agreement was modest in the “gray zone.” In these challenging cases, the use of quantitation may help to detect subtle amyloid accumulation. The appropriate definition of a “gray zone” can

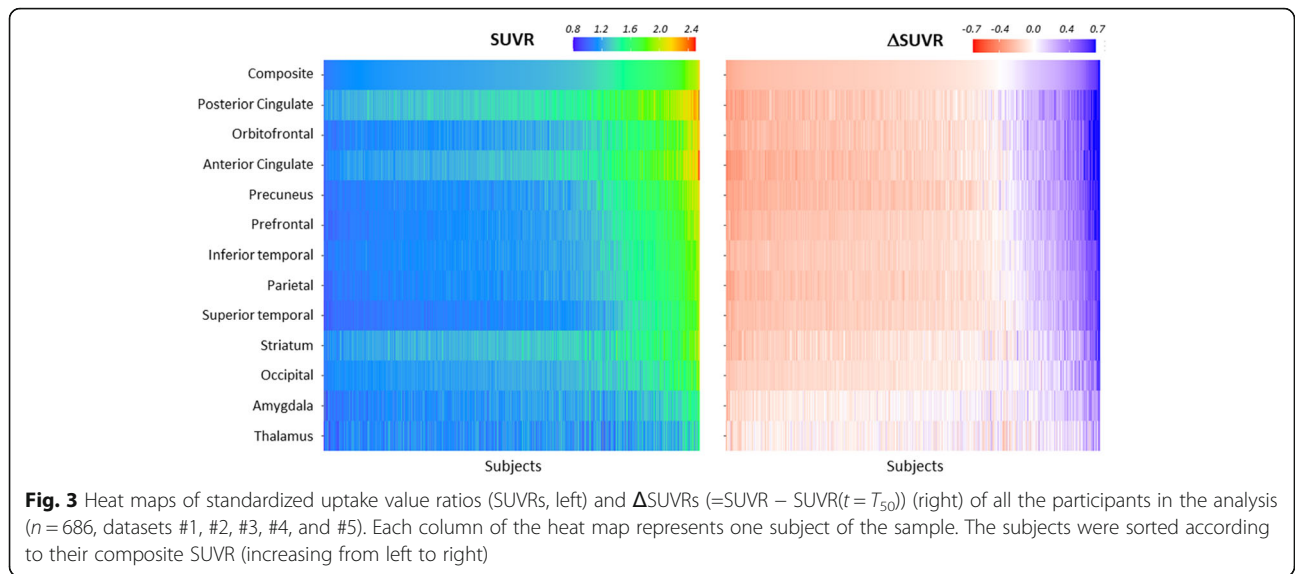
improve the detection of emerging A β pathology in observational, prevention, and therapeutic trials and is key for the screening of asymptomatic population in clinical trials and detection of subjects that will likely accumulate amyloid. Subjects having amyloid values in the gray zone may be the most likely to respond to pharmacological or non-pharmacological interventions because they have early evidence of disease without the cognitive deficits and neuronal loss that signifies AD.

This study is in agreement with a number of recent reports across different tracers converging to the utility of using two cutoffs for amyloid PET abnormality, an early cutoff around CL = 11–17 where pathology may be emerging, and a second around CL = 29–36 where amyloid burden levels correspond to moderate and frequent neuritic plaques (CERAD stages B–C, [33]) by neuropathology. Early cutoffs of 11, 14, and

Table 3 SUVRs of eHC ($n = 66$) and AD subjects ($n = 73$) (dataset #2) and cutoffs for the detection of established A β pathology

Method	Region	SUVR _{eHC}	SUVR _{AD}	SUVR _{cutoff}	Sensitivity	Specificity	AUC
MRI-based ROIs	Frontal	1.15 ± 0.07	1.57 ± 0.19	1.31	95%	97%	0.98
	Lateral temporal	1.15 ± 0.05	1.51 ± 0.17	1.26	97%	98%	0.96
	Occipital	1.20 ± 0.06	1.43 ± 0.16	1.29	88%	95%	0.94
	Parietal	1.13 ± 0.08	1.51 ± 0.16	1.26	97%	98%	0.98
	Anterior cingulate	1.28 ± 0.09	1.70 ± 0.22	1.43	92%	97%	0.98
	Posterior cingulate	1.33 ± 0.09	1.77 ± 0.21	1.47	93%	97%	0.97
	Precuneus	1.15 ± 0.08	1.60 ± 0.19	1.28	95%	98%	0.98
	Composite	1.21 ± 0.06	1.58 ± 0.17	1.38	93%	100%	0.98
CL ROIs	Cortex	1.05 ± 0.06	1.54 ± 0.22	1.24	95%	100%	0.98
		6.8 ± 8.8 CL	81.0 ± 33.2 CL	35.7 CL			

eHC elderly healthy controls, A β amyloid-beta, SUVR_{eHC} SUVR (mean ± SD) of the elderly healthy controls, SUVR_{AD} SUVR (mean ± SD) of the Alzheimer's disease patients, AUC area under the receiver operating curve, SUVR_{cutoff} SUVR cutoff obtained from the ROC analysis using visual assessment as standard of truth, MRI magnetic resonance imaging, ROI region of interest, CL centiloid



17 CL have been reported for the FACEHBI, ALFA+, and AMYPAD Prognostic and Natural History Study studies using Gaussian mixture models [34]. Similarly, Salvadó et al. identified two cutoffs based on a direct comparison with established CSF A β 42 thresholds: CL = 12 to rule out-amyloid pathology and CL = 29 to

denote established pathology [35]. Mormino et al. also showed the biological relevance of slight ^{11}C -PIB elevations in elderly normal control subjects and provided an estimate for the cutoffs defining the “gray zone” using distribution volume ratios [36]. Finally, La Joie et al. and Doré et al. reported using

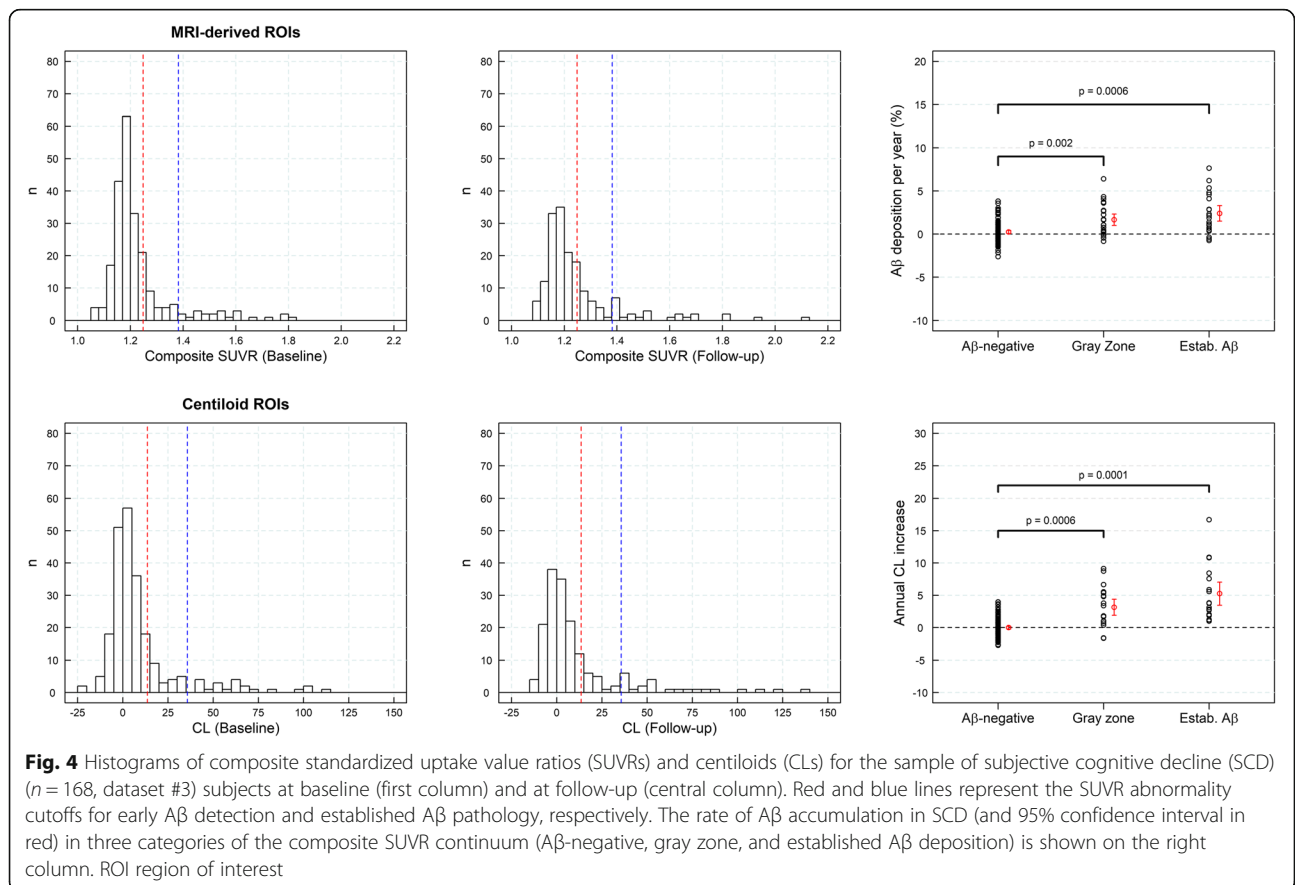


Table 4 Regional percent of Aβ deposition per year in a sample of subject with SCD (n = 168, dataset #3)

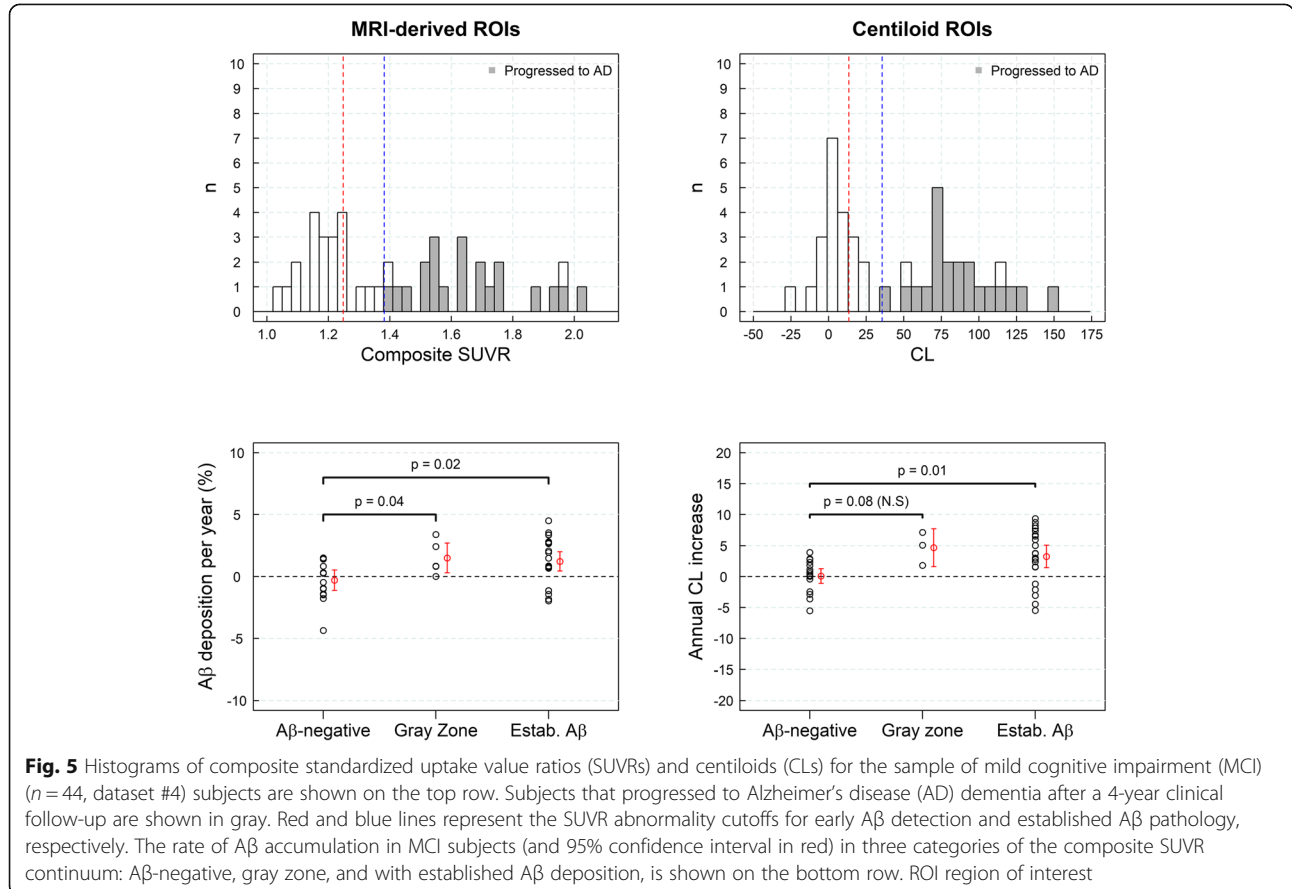
Method	Region	Percent Aβ deposition per year		
		Aβ-negative	Gray zone	Established Aβ pathology
MRI-based ROIs	Frontal	-0.01 ± 1.15 (p = 0.52)	1.08 ± 1.91 (p < 10 ⁻³)	2.72 ± 2.53 (p < 10 ⁻⁴)
	Lateral temporal	0.08 ± 0.99 (p = 0.21)	1.07 ± 1.61 (p < 10 ⁻⁴)	2.05 ± 2.18 (p < 10 ⁻³)
	Occipital	0.36 ± 1.13 (p < 10 ⁻³)	0.50 ± 1.74 (p = 0.38)	1.85 ± 2.18 (p < 10 ⁻³)
	Parietal	0.12 ± 1.29 (p = 0.16)	1.39 ± 2.10 (p = 0.02)	2.61 ± 2.28 (p < 10 ⁻⁵)
	Anterior cingulate	0.17 ± 1.81 (p = 0.13)	1.42 ± 2.12 (p = 0.10)	2.37 ± 3.07 (p = 0.001)
	Posterior cingulate	0.71 ± 1.72 (p < 10 ⁻⁵)	N.A	3.14 ± 2.46 (p < 10 ⁻⁷)
	Precuneus	0.31 ± 1.37 (p = 0.006)	N.A	N.A
	Composite	0.24 ± 1.24 (p = 0.02)	1.66 ± 1.86 (p < 10 ⁻³)	2.40 ± 2.37 (p < 10 ⁻³)
CL	Cortex	0.00 ± 0.89 (p = 0.53)	1.81 ± 1.86 (p < 10 ⁻³)	2.38 ± 1.82 (p < 10 ⁻⁴)

SCD subjective cognitive decline, N.A not available (As Aβ-negative, gray zone, and established Aβ pathology were defined regionally using cutoffs reported in Tables 2 and 3, there were not enough regional standardized uptake values (SUVRs) to calculate percent Aβ deposition per year in some regions), Aβ amyloid-beta, MRI magnetic resonance imaging, ROI region of interest, CL centiloid. p-values testing whether percent Aβ deposition per year is significantly larger than zero are given in parenthesis

histopathological confirmation gray zones from 12.2–24.4 and 19–28 CLs, respectively [17, 37].

This study also showed that topographical information can help identify increased signal earlier than traditional global cutoffs, with cingulate cortices (anterior and posterior), precuneus, and orbitofrontal cortices being the first regions to show pathological tracer retention,

followed by prefrontal, inferior lateral temporal parietal, and occipital cortices. These results agree with previous publications using PET where precuneus, cingulate, and frontal cortices displayed higher PET signal earlier than the remaining neocortical regions [38–40]. However, recent publications suggest that other regions such as the banks of the superior temporal, not analyzed in this



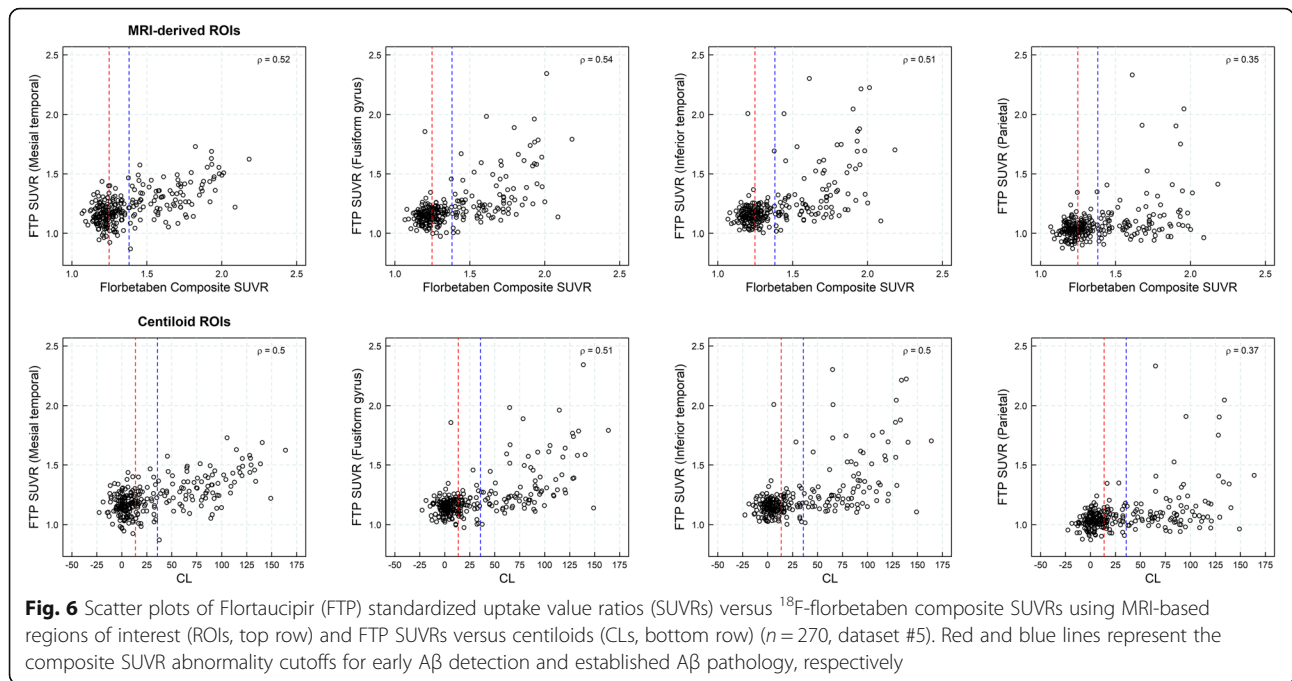


Fig. 6 Scatter plots of Flortaucipir (FTP) standardized uptake value ratios (SUVRs) versus ¹⁸F-florbetaben composite SUVRs using MRI-based regions of interest (ROIs, top row) and FTP SUVRs versus centiloids (CLs, bottom row) (*n* = 270, dataset #5). Red and blue lines represent the composite SUVR abnormality cutoffs for early Aβ detection and established Aβ pathology, respectively

article, may also show early Aβ deposition and subjects with high Aβ in these regions are at increased risk of cognitive decline [41]. Even though regions with “early” amyloid have been identified in this work, these early elevations are subtle, occasionally may not be detectable at the individual level and the amyloid PET signal is highly correlated across all regions. These subtle differences across regions are consistent with some articles reporting that a sigmoidal model fitting amyloid deposition with the same *T*₅₀ across brain regions is optimal [32]. In addition, amyloid PET is affected by several technical factors such as the type of camera used, reconstruction methods, corrections applied (e.g., partial

volume effect), and quantitative methods used that may have an impact on the regional SUVR estimates. For this reason, topographically defined distribution and early Aβ accumulation measured by PET may not necessarily agree with histopathology findings. Despite these discrepancies with neuropathology results, several studies have shown the utility of amyloid PET topographical quantification in staging AD [21–23], determining the risk of subsequent cognitive decline [23, 25], optimal subject selection for anti-amyloid interventional trials [22, 42], and reducing sample size in anti-amyloid interventional trials [43, 44]. Pascoal et al. also showed that the topographical pattern of individuals with MCI that

Table 5 Regional percent of Aβ deposition per year in a sample of MCI subjects (*n* = 44, dataset #4)

Method	Region	Percent Aβ deposition per year		
		Aβ-negative	Gray zone	Established Aβ pathology
MRI-based ROIs	Frontal	-0.49 ± 2.52 (<i>p</i> = 0.73)	0.85 ± 2.20 (<i>p</i> = 0.19)	1.37 ± 2.02 (<i>p</i> = 0.002)
	Lateral temporal	0.15 ± 1.83 (<i>p</i> = 0.40)	0.88 ± 1.58 (<i>p</i> = 0.08)	1.66 ± 1.90 (<i>p</i> < 10 ⁻³)
	Occipital	0.30 ± 1.64 (<i>p</i> = 0.21)	0.24 ± 1.78 (<i>p</i> = 0.44)	0.94 ± 2.28 (<i>p</i> = 0.055)
	Parietal	-0.48 ± 1.72 (<i>p</i> = 0.87)	1.39 ± 1.23 (<i>p</i> = 0.09)	1.12 ± 1.88 (<i>p</i> = 0.009)
	Anterior cingulate	-0.79 ± 2.49 (<i>p</i> = 0.87)	0.97 ± 0.22 (<i>p</i> = 0.01)	0.76 ± 2.51 (<i>p</i> = 0.08)
	Posterior cingulate	0.71 ± 1.41 (<i>p</i> = 0.04)	N.A	1.58 ± 2.26 (<i>p</i> = 0.001)
	Precuneus	0.01 ± 1.37 (<i>p</i> = 0.49)	1.24 ± 1.56 (<i>p</i> = 0.11)	1.44 ± 2.31 (<i>p</i> = 0.004)
	Composite	-0.29 ± 1.68 (<i>p</i> = 0.74)	1.51 ± 1.38 (<i>p</i> = 0.04)	1.23 ± 1.90 (<i>p</i> = 0.004)
CL	Cortex	0.08 ± 1.62 (<i>p</i> = 0.43)	2.62 ± 1.47 (<i>p</i> = 0.045)	1.41 ± 1.82 (<i>p</i> = 0.001)

MCI mild cognitive impairment, N.A not available (As Aβ-negative, gray zone, and established Aβ pathology were defined regionally using cutoffs reported in Tables 2 and 3, there were not enough regional standardized uptake values (SUVRs) to calculate percent Aβ deposition per year in some regions), Aβ amyloid-beta, MRI magnetic resonance imaging, ROI region of interest, CL centiloid. *p*-values testing whether percent Aβ deposition per year is significantly larger than zero are given in parenthesis

Table 6 Regional ¹⁸F-flortaucipir SUVRs by amyloid group (n = 270, dataset #5)

Method	Region	¹⁸ F-Flortaucipir SUVR		
		Aβ-negative	Gray zone	Established Aβ pathology
MRI-based ROI	Mesial temporal	1.16 ± 0.09	1.18 ± 0.10 (p = 0.51)	1.32 ± 0.15 (p < 10 ⁻⁵)
	Fusiform gyrus	1.15 ± 0.09	1.16 ± 0.08 (p = 0.91)	1.34 ± 0.24 (p < 10 ⁻⁵)
	Inferior temporal	1.15 ± 0.10	1.17 ± 0.10 (p = 0.87)	1.32 ± 0.15 (p < 10 ⁻⁵)
	Parietal	1.03 ± 0.07	1.05 ± 0.07 (p = 0.58)	1.15 ± 0.23 (p < 10 ⁻⁵)
CL	Mesial temporal	1.16 ± 0.09	1.18 ± 0.11 (p = 0.45)	1.33 ± 0.15 (p < 10 ⁻⁵)
	Fusiform gyrus	1.15 ± 0.08	1.16 ± 0.09 (p = 0.88)	1.35 ± 0.24 (p < 10 ⁻⁵)
	Inferior temporal	1.15 ± 0.05	1.18 ± 0.11 (p = 0.60)	1.38 ± 0.28 (p < 10 ⁻⁵)
	Parietal	1.03 ± 0.06	1.06 ± 0.09 (p = 0.37)	1.16 ± 0.24 (p < 10 ⁻⁵)

SUVR ¹⁸F-flortaucipir SUVRs (mean ± SD), Aβ amyloid-beta, MRI magnetic resonance imaging, ROI region of interest, CL centiloid. p-values using ANOVA to test whether ¹⁸F-flortaucipir SUVRs in each group are significantly larger than in Aβ-negative subjects are given in parenthesis

progress to dementia is “traditionally AD-like,” while that of non-converters includes more temporal and occipital regions instead [24]. In this regard, even though CL ROIs and composite SUVR from MRI-derived ROIs provided overall similar results when determining subject in the “gray zone,” the use of CL and composite

SUVR is limited in determining the topographical distribution of Aβ load.

As a limitation of this study, it should be mentioned that SUVR cutoff for the detection of established amyloid pathology was derived using visual assessment as a standard of truth and this may bias the proportion of

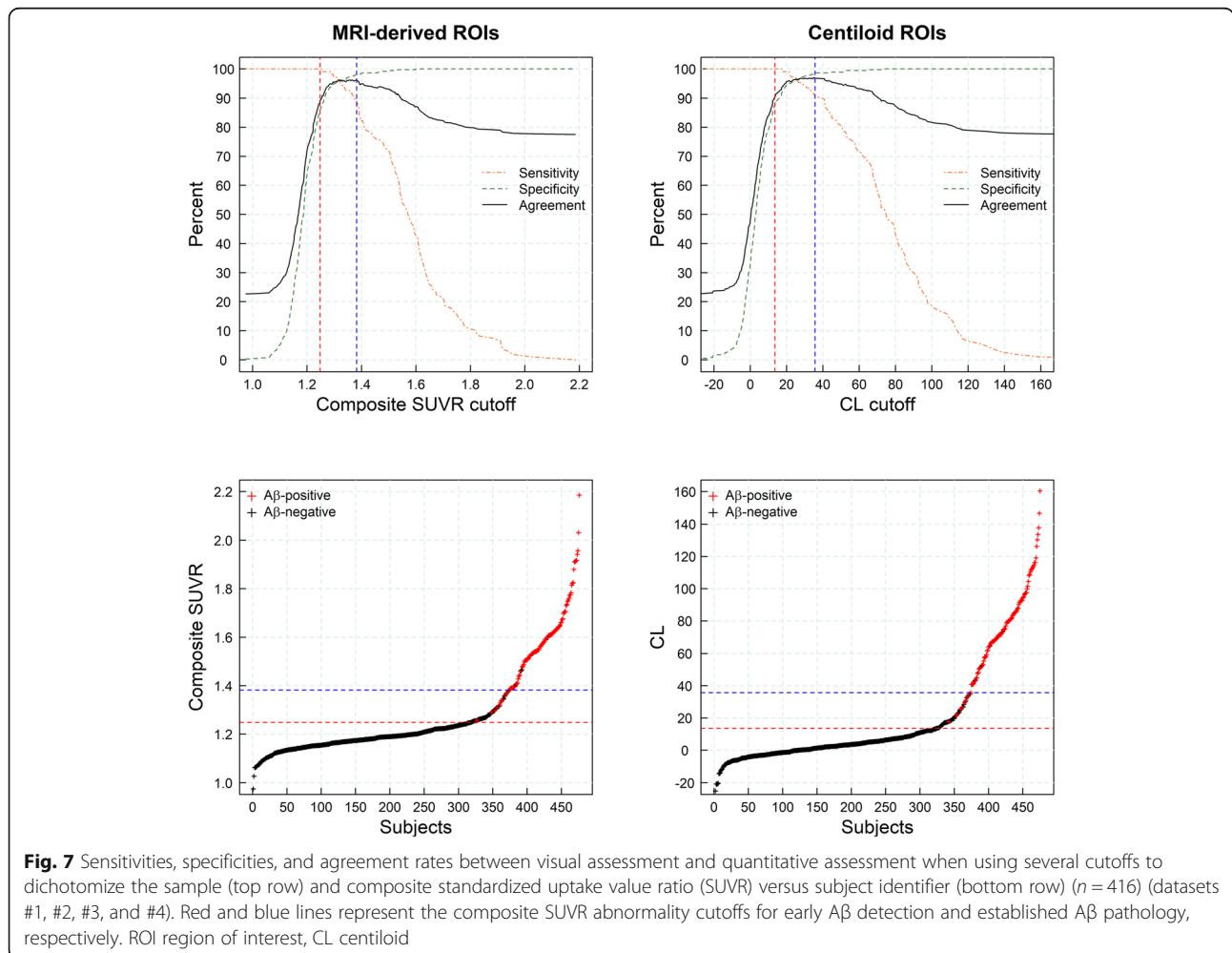


Fig. 7 Sensitivities, specificities, and agreement rates between visual assessment and quantitative assessment when using several cutoffs to dichotomize the sample (top row) and composite standardized uptake value ratio (SUVR) versus subject identifier (bottom row) (n = 416) (datasets #1, #2, #3, and #4). Red and blue lines represent the composite SUVR abnormality cutoffs for early Aβ detection and established Aβ pathology, respectively. ROI region of interest, CL centiloid

visually positive scans per group. To clarify this potential bias, a Gaussian mixture model was fitted to the whole population of the study (datasets #1, #2, #3, #4, and #5) confirming the cutoffs previously reported in the manuscript (14 and 32 CL), proportion of positive scans per group and accurate definition of the “gray zone” (supplemental material 2). A second limitation is that SUVR may be biased as a surrogate marker of A β load by changes in cerebral blood flow (CBF) or radiotracer clearance [45] and SUVR cutoffs may depend on methodological aspects such as equipment, reconstruction, imaging window, image processing, smoothing, and corrections applied. To minimize this methodological limitation, a harmonization procedure was applied to convert all the images into a common resolution as described in Joshi et al. [27]. Even so, the application of cutoffs developed here should be applied with caution to studies using different methods or non-harmonized data.

Conclusions

This study supports the utility of two cutoffs for ¹⁸F-florbetaben amyloid PET abnormality defining a “gray zone”: a first cutoff of 13.5 CL that indicated emerging A β pathology and a second cutoff of 35.7 CL where amyloid burden levels correspond to established AD neuropathology findings. These cutoffs define a subset of subjects characterized by pre-AD dementia levels of amyloid burden that may precede the alteration of other biomarkers such as tau deposition or clinical symptoms and accelerated amyloid accumulation. Amyloid PET images in the “gray zone” are more likely to be ambiguous by the current binary global visual assessment methodology. At the MCI stage, the determination of different amyloid loads, particularly low amyloid levels, is useful in determining who will eventually progress to dementia. Quantitation of amyloid provides a sensitive measure in these low-load cases and may help to identify a group of subjects most likely to benefit from intervention.

Supplementary Information

Supplementary information accompanies this paper at <https://doi.org/10.1186/s13195-021-00807-6>.

Additional file 1.

Additional file 2.

Acknowledgements

The FACEHBI study group: Abdelnour C^{1,2}, Aguilera N¹, Alarcón-Martín E¹, Alegret M^{1,2}, Alonso-Lana S¹, Berthier M³, Buendía M¹, Campos F⁴, Cañabate P^{1,2}, Cañada L¹, Cuevas C¹, de Rojas J¹, Diego S¹, Espinosa A^{1,2}, Esteban-De Antonio E¹, Gailhajianet A¹, García P¹, Giménez J⁵, Gómez-Chiari M⁵, Guitart M¹, Hernández I^{1,2}, Ibarria, M¹, Lafuente A¹, Lomeña F⁴, López-Cuevas R¹, Masip E¹, Martín E¹, Martínez J¹, Mauleón A¹, Moreno M¹, Moreno-Grau S^{1,2}, Montreal L¹, Niñerola A⁴, Nogales AB¹, Núñez L⁶, Orellana A¹, Ortega G¹, Páez A⁶, Pancho A¹, Pelejà E¹, Pérez-Cordon A¹, Pérez-Grijalba V⁷, Perissinotti

A⁴, Pesini P⁷, Preckler S¹, Roberto N¹, Romero J⁷, Ramis M¹, Rosende-Roca M¹, Ruiz A^{1,2}, Sarasa M⁷, Tejero MA⁵, Torres M⁶, Valero S^{1,2}, Vargas L¹, Vivas A⁵. ¹Fundacio ACE Institut Català de Neurociències Aplicades, Research Center and Memory Unit – Universitat Internacional de Catalunya. Barcelona, Spain; ²CIBERNED, Center for Networked Biomedical Research on Neurodegenerative Diseases, National Institute of Health Carlos III, Ministry of Economy and Competitiveness, Spain. ³Cognitive Neurology and Aphasia Unit (UNCA). University of Malaga. ⁴Servei de Medicina Nuclear, Hospital Clínic i Provincial, Barcelona, Spain; ⁵Departament de Diagnòstic per la Imatge. Clínica Corachan, Barcelona, Spain; ⁶Grifols®, ⁷Araclon Biothec®. Zaragoza, Spain).

Authors' contributions

All authors made a substantial contribution in interpreting of the study results and revising the manuscript critically for important intellectual content and approved the final version to be published. SB and NRV performed image and statistical analysis and prepared the first versions of the manuscript. SB, NRV, NK, AM, AP, AJ, SDS, and AS contributed to the concept, design, and interpretation of the study. W, VD, and CR participated in the acquisition and interpretation of data from MCI subjects MM, AS, JPT, OSG, LT, and MB participated in the acquisition and interpretation of results from subjective memory complainers (FACEHBI study). HB and OS participated in the acquisition and interpretation of results from elderly HC and AD subjects. JS participated in the acquisition and interpretation of results from the young healthy volunteers. SML participated in the interpretation of results from the young healthy volunteers and ADNI participants.

Authors' information

Authors are on behalf of the AMYPAD consortium: Santiago Bullich, Núria Roé-Vellvé, Marta Marquí, Àngela Sanabria, Juan Pablo Tartari, Oscar Sotolongo-Grau, Norman Koglin, Andre Müller, Audrey Perrotin, Aleksandar Jovalekic, Lluís Tàrraga, Andrew W. Stephens, Mercè Boada.

Authors are on behalf of the FACEHBI study group: Marta Marquí, Àngela Sanabria, Juan Pablo Tartari, Oscar Sotolongo-Grau, Lluís Tàrraga, Mercè Boada.

Funding

Part of the data were acquired in clinical studies funded by Bayer Pharma AG or Piramal Imaging.

Part of the data collection and sharing for this project was funded by the Alzheimer's Disease Neuroimaging Initiative (ADNI) (National Institutes of Health Grant U01 AG024904) and DOD ADNI (Department of Defense award number W81XWH-12-2-0012). ADNI is funded by the National Institute on Aging, the National Institute of Biomedical Imaging and Bioengineering, and through generous contributions from the following: AbbVie, Alzheimer's Association; Alzheimer's Drug Discovery Foundation; Araclon Biotech; BioClinica, Inc.; Biogen; Bristol-Myers Squibb Company; CereSpir, Inc.; Cogstate; Eisai Inc.; Elan Pharmaceuticals, Inc.; Eli Lilly and Company; EuroImmun; F. Hoffmann-La Roche Ltd. and its affiliated company Genentech, Inc.; Fujirebio; GE Healthcare; IXICO Ltd.; Janssen Alzheimer Immunotherapy Research & Development, LLC.; Johnson & Johnson Pharmaceutical Research & Development LLC.; Lumosity; Lundbeck; Merck & Co., Inc.; Meso Scale Diagnostics, LLC.; NeuroRx Research; Neurotrack Technologies; Novartis Pharmaceuticals Corporation; Pfizer Inc.; Piramal Imaging; Servier; Takeda Pharmaceutical Company; and Transition Therapeutics. The Canadian Institutes of Health Research is providing funds to support ADNI clinical sites in Canada. Private sector contributions are facilitated by the Foundation for the National Institutes of Health (www.fnih.org). The grantee organization is the Northern California Institute for Research and Education, and the study is coordinated by the Alzheimer's Therapeutic Research Institute at the University of Southern California. ADNI data are disseminated by the Laboratory for Neuro Imaging at the University of Southern California.

Part of the data used in the preparation of this article were obtained from the Alzheimer's Disease Neuroimaging Initiative (ADNI) database (adni.loni.usc.edu). As such, the investigators within the ADNI contributed to the design and implementation of ADNI and/or provided data but did not participate in the analysis or writing of this report. A complete listing of ADNI investigators can be found at http://adni.loni.usc.edu/wp-content/uploads/how_to_apply/ADNI_Acknowledgement_List.pdf

The FACEHBI study was supported by funds from Fundació ACE Institut Català de Neurociències Aplicades, Grifols, Life Molecular Imaging, Araclon Biotech, Alkahest, Laboratorio de análisis Echevarne, and IrsiCaixa. This work has received support from the EU-EFPIA Innovative Medicines Initiatives 2 Joint Undertaking (grant no. 115952). This communication reflects the views of the authors and neither IML nor the European Union and EFPIA are liable for any use that may be made of the information contained herein.

Availability of data and materials

The datasets generated and/or analyzed during the current study are not publicly available.

Declarations

Ethics approval and consent to participate

All studies were conducted in accordance with the Declaration of Helsinki and after approval of the local ethics committees of the participating centers. All participants (or their legal representatives) provided written informed consent prior to recruitment.

Consent for publication

Not applicable.

Competing interests

SB, NRV, NK, AM, AP, AJ, and AS are employees of Life Molecular Imaging GmbH (formerly Piramal Imaging GmbH). SDS is an employee of Eisai Inc. and a former employee of Life Molecular Imaging Inc. (formerly Piramal Pharma Inc). HB and OS received research support, consultant honoraria, and travel expenses from Piramal Imaging GmbH. Victor L. Villemagne has received speaker's honoraria from Piramal Imaging, GE Healthcare, Avid Pharmaceuticals, AstraZeneca, and Hoffmann-La Roche and consulting fees for Novartis, Lundbeck, Abbvie, Shanghai Green Valley Pharmaceutical Co. LTD, and Hoffmann-La Roche. Christopher C. Rowe has received research grants from Bayer Schering Pharma, Piramal Imaging, Avid Radiopharmaceuticals, Navidea, GE Healthcare, AstraZeneca, and Biogen. John Seibyl holds equity in Invicro and consulting fees from LMI, Roche, Biogen, Abvie, and Invicro. M. Boada has received research funds from the following private donors: Grifols SA, CaixaBank S.A., Piramal Imaging, Araclon Biotech, Laboratorios Echevarne, Fundació Castell de Peralada, and Fundació La Pedrera and has participated in advisory boards of Araclon Biotech, Biogen, Bioibérica, Eisai, Grifols, Lilly, Merck, Nutricia, Roche, Schwabe Farma, Servier, and Kyowa Kirin.

No other potential conflict of interest relevant to this article was reported.

Author details

¹Life Molecular Imaging GmbH, Tegeler Str. 6-7, 13353 Berlin, Germany. ²Fundació ACE Institut Català de Neurociències Aplicades, Research Center and Memory Unit - Universitat Internacional de Catalunya (UIC), Barcelona, Spain. ³Centro de Investigación Biomédica en Red Enfermedades Neurodegenerativas (CIBERNED), Instituto de Salud Carlos III, Madrid, Spain. ⁴Helen Willis Neuroscience Institute, University of California, Berkeley and Lawrence Berkeley National Laboratory, Berkeley, CA, USA. ⁵Department of Nuclear Medicine, University Hospital Leipzig, Leipzig, Germany. ⁶Department of Psychiatry, University of Pittsburgh, Pittsburgh, PA, USA. ⁷Departments of Medicine and Molecular Imaging, University of Melbourne, Austin Health, Melbourne, Victoria, Australia. ⁸The Australian e-Health Research Centre, Health and Biosecurity, CSIRO, Melbourne, Victoria, Australia. ⁹Life Molecular Imaging Inc, Boston, MA, USA. ¹⁰Invicro, New Haven, CT, USA.

Received: 23 December 2020 Accepted: 10 March 2021

Published online: 27 March 2021

References

- Braak H, Braak E. Frequency of stages of Alzheimer-related lesions in different age categories. *Neurobiol Aging*. 1997;18(4):351–7.
- Villemagne VL, Burnham S, Bourgeat P, Brown B, Ellis KA, Salvado O, et al. Amyloid beta deposition, neurodegeneration, and cognitive decline in sporadic Alzheimer's disease: a prospective cohort study. *Lancet Neurol*. 2013;12(4):357–67.
- Blennow K, Zetterberg H, Rinne JO, Salloway S, Wei J, Black R, et al. Effect of immunotherapy with bapineuzumab on cerebrospinal fluid biomarker levels in patients with mild to moderate Alzheimer disease. *Arch Neurol*. 2012;69(8):1002–10.
- Uenaka K, Nakano M, Willis BA, Friedrich S, Ferguson-Sells L, Dean RA, et al. Comparison of pharmacokinetics, pharmacodynamics, safety, and tolerability of the amyloid beta monoclonal antibody solanezumab in Japanese and white patients with mild to moderate Alzheimer disease. *Clin Neuropharmacol*. 2012;35(1):25–9.
- Weninger S, Carrillo MC, Dunn B, Aisen PS, Bateman RJ, Kotz JD, et al. Collaboration for Alzheimer's prevention: principles to guide data and sample sharing in preclinical Alzheimer's disease trials. *Alzheimers Dement*. 2016;12(5):631–2.
- McDade E, Bateman RJ. Stop Alzheimer's before it starts. *Nature*. 2017;547(7662):153–5.
- Ritchie CW, Molinuevo JL, Truyen L, Satlin A, Van der Geyten S, Lovestone S. Development of interventions for the secondary prevention of Alzheimer's dementia: the European Prevention of Alzheimer's Dementia (EPAD) project. *Lancet Psychiatry*. 2016;3(2):179–86.
- Sperling RA, Jack CR Jr, Aisen PS. Testing the right target and right drug at the right stage. *Sci Transl Med*. 2011;3(111):111cm33.
- Sabri O, Sabbagh MN, Seibyl J, Barthel H, Akatsu H, Ouchi Y, et al. Florbetaben PET imaging to detect amyloid beta plaques in Alzheimer's disease: phase 3 study. *Alzheimers Dement*. 2015;11(8):964–74.
- Seibyl J, Catafau AM, Barthel H, Ishii K, Rowe CC, Leverenz JB, et al. Impact of training method on the robustness of the visual assessment of 18F-florbetaben PET scans: results from a phase-3 study. *J Nucl Med*. 2016;57(6):900–6.
- Bullich S, Villemagne VL, Catafau AM, Jovalekic A, Koglin N, Rowe CC, et al. Optimal reference region to measure longitudinal amyloid-beta change with ¹⁸F-florbetaben PET. *J Nucl Med*. 2017;58(8):1300–6.
- Bullich S, Seibyl J, Catafau AM, Jovalekic A, Koglin N, Barthel H, et al. Optimized classification of ¹⁸F-florbetaben PET scans as positive and negative using an SUVR quantitative approach and comparison to visual assessment. *Neuroimage Clin*. 2017;15:325–32.
- Barthel H, Gertz HJ, Dresel S, Peters O, Bartenstein P, Buerger K, et al. Cerebral amyloid-beta PET with florbetaben (18F) in patients with Alzheimer's disease and healthy controls: a multicentre phase 2 diagnostic study. *Lancet Neurol*. 2011;10(5):424–35.
- Jennings D, Seibyl J, Sabbagh M, Lai F, Hopkins W, Bullich S, et al. Age dependence of brain beta-amyloid deposition in Down syndrome: an [18F] florbetaben PET study. *Neurology*. 2015;84(5):500–7.
- Tuszynski T, Rullmann M, Luthardt J, Butzke D, Tiepolt S, Gertz HJ, et al. Evaluation of software tools for automated identification of neuroanatomical structures in quantitative beta-amyloid PET imaging to diagnose Alzheimer's disease. *Eur J Nucl Med Mol Imaging*. 2016;43(6):1077–87.
- Villemagne VL, Ong K, Mulligan RS, Holl G, Pejoska S, Jones G, et al. Amyloid imaging with (18F)-florbetaben in Alzheimer disease and other dementias. *J Nucl Med*. 2011;52(8):1210–7.
- Doré V, Bullich S, Rowe CC, Bourgeat P, Konate S, Sabri O, et al. Comparison of ¹⁸F-florbetaben quantification results using the standard centiloid, MR-based, and MR-less CapAIBL(R) approaches: validation against histopathology. *Alzheimers Dement*. 2019;15(6):807–16.
- Ong K, Villemagne VL, Bahar-Fuchs A, Lamb F, Chételat G, Raniga P, et al. (18F)-florbetaben Abeta imaging in mild cognitive impairment. *Alzheimers Res Ther*. 2013;5(1):4.
- Bischof GN, Jacobs HIL. Subthreshold amyloid and its biological and clinical meaning: long way ahead. *Neurology*. 2019;93(2):72–9.
- Fantoni E, Collij L, Lopes Alves I, Buckley C, Farrar G. AMYPAD consortium. The spatial-temporal ordering of amyloid pathology and opportunities for PET imaging. *J Nucl Med*. 2020;61(2):166–71.
- Grothe MJ, Barthel H, Sepulcre J, Dyrba M, Sabri O, Teipel SJ. In vivo staging of regional amyloid deposition. *Neurology*. 2017;89(20):2031–8.
- Mattsson N, Palmqvist S, Stomrud E, Vogel J, Hansson O. Staging beta-amyloid pathology with amyloid positron emission tomography. *JAMA Neurol*. 2019;76(11):1319–29.
- Collij LE, Heeman F, Salvadó G, Ingala S, Altomare D, de Wilde A, et al. Multitracer model for staging cortical amyloid deposition using PET imaging. *Neurology*. 2020;95(11):e1538–53.
- Pascoal TA, Therriault J, Mathotaarachchi S, Kang MS, Shin M, Benedet AL, et al. Topographical distribution of Abeta predicts progression to dementia in Abeta positive mild cognitive impairment. *Alzheimers Dement (Amst)*. 2020;12(1):e12037.

25. Hanseeuw BJ, Betensky RA, Mormino EC, Schultz AP, Sepulcre J, Becker JA, et al. PET staging of amyloidosis using striatum. *Alzheimers Dement*. 2018; 14(10):1281–92.
26. Rodríguez-Gomez O, Sanabria A, Perez-Cordon A, Sanchez-Ruiz D, Abdelnour C, Valero S, et al. FACEHBI: a prospective study of risk factors, biomarkers and cognition in a cohort of individuals with subjective cognitive decline. Study rationale and research protocols. *J Prev Alzheimers Dis*. 2017;4(2):100–8.
27. Joshi A, Koeppe RA, Fessler JA. Reducing between scanner differences in multi-center PET studies. *Neuroimage*. 2009;46(1):154–9.
28. Tzourio-Mazoyer N, Landeau B, Papathanassiou D, Crivello F, Etard O, Delcroix N, et al. Automated anatomical labeling of activations in SPM using a macroscopic anatomical parcellation of the MNI MRI single-subject brain. *Neuroimage*. 2002;15(1):273–89.
29. Rowe CC, Ackerman U, Browne W, Mulligan R, Pike KL, O'Keefe G, et al. Imaging of amyloid beta in Alzheimer's disease with 18F-BAY94-9172, a novel PET tracer: proof of mechanism. *Lancet Neurol*. 2008;7(2):129–35.
30. Klunk WE, Koeppe RA, Price JC, Benzinger TL, Devous MD Sr, Jagust WJ, et al. The Centiloid Project: standardizing quantitative amyloid plaque estimation by PET. *Alzheimers Dement*. 2015;11(1):1–15 e1–4.
31. Rowe CC, Doré V, Jones G, Baxendale D, Mulligan RS, Bullich S, et al. ¹⁸F-Florbetaben PET beta-amyloid binding expressed in centiloids. *Eur J Nucl Med Mol Imaging*. 2017;44(12):2053–9.
32. Whittington A, Sharp DJ, Gunn RN. Spatiotemporal distribution of β -amyloid in Alzheimer disease is the result of heterogeneous regional carrying capacities. *J Nucl Med*. 2018;59(5):822–7.
33. Mirra SS, Heyman A, McKeel D, Sumi SM, Crain BJ, Brownlee LM, et al. The Consortium to Establish a Registry for Alzheimer's Disease (CERAD). Part II. Standardization of the neuropathologic assessment of Alzheimer's disease. *Neurology*. 1991;41:479–86.
34. Bullich S. Converging evidence for a “gray-zone” of amyloid burden and its relevance. in AALC. 2020. Virtual.
35. Salvadó G, Molinuevo JL, Brugulat-Serrat A, Falcon C, Grau-Rivera O, Suárez-Calvet M, et al. Centiloid cut-off values for optimal agreement between PET and CSF core AD biomarkers. *Alzheimers Res Ther*. 2019;11(1):27.
36. Mormino EC, Brandel MG, Madison CM, Rabinovici GD, Marks S, Baker SL, et al. Not quite PIB-positive, not quite PIB-negative: slight PIB elevations in elderly normal control subjects are biologically relevant. *Neuroimage*. 2012; 59(2):1152–60.
37. La Joie R, Ayakta N, Seeley WW, Borys E, Boxer AL, DeCarli C, et al. Multisite study of the relationships between antemortem [¹¹C]PIB-PET Centiloid values and postmortem measures of Alzheimer's disease neuropathology. *Alzheimers Dement*. 2019;15(2):205–16.
38. Villeneuve S, Rabinovici GD, Cohn-Sheehy BI, Madison C, Ayakta N, Ghosh PM, et al. Existing Pittsburgh Compound-B positron emission tomography thresholds are too high: statistical and pathological evaluation. *Brain*. 2015; 138(Pt 7):2020–33.
39. Cho H, Choi JY, Hwang MS, Kim YJ, Lee HM, Lee HS, et al. In vivo cortical spreading pattern of tau and amyloid in the Alzheimer disease spectrum. *Ann Neurol*. 2016;80(2):247–58.
40. Palmqvist S, Schöll M, Strandberg O, Mattsson N, Stomrud E, Zetterberg H, et al. Earliest accumulation of β -amyloid occurs within the default-mode network and concurrently affects brain connectivity. *Nat Commun*. 2017;8(1):1214.
41. Guo T, Landau SM, Jagust WJ. Detecting earlier stages of amyloid deposition using PET in cognitively normal elderly adults. *Neurology*. 2020; 94(14):e1512–24.
42. Guo T, Dukart J, Brendel M, Rominger A, Grimmer T, Yakushev I. Rate of beta-amyloid accumulation varies with baseline amyloid burden: implications for anti-amyloid drug trials. *Alzheimers Dement*. 2018;14(11):1387–96.
43. Insel PS, Mormino EC, Aisen PS, Thompson WK, Donohue MC. Neuroanatomical spread of amyloid beta and tau in Alzheimer's disease: implications for primary prevention. *Brain Commun*. 2020;2(1):fcaa007.
44. Lopes Alves I, Collij LE, Altomare D, Frisoni GB, Saint-Aubert L, Payoux P, et al. Quantitative amyloid PET in Alzheimer's disease: the AMYPAD prognostic and natural history study. *Alzheimers Dement*. 2020;16(5):750–8.
45. Bullich S, Barthel H, Koglin N, Becker GA, De Santi S, Jovalekic A, et al. Validation of noninvasive tracer kinetic analysis of (18)F-Florbetaben PET using a dual-time-window acquisition protocol. *J Nucl Med*. 2018;59(7):1104–10.

Publisher's Note

Springer Nature remains neutral with regard to jurisdictional claims in published maps and institutional affiliations.

Ready to submit your research? Choose BMC and benefit from:

- fast, convenient online submission
- thorough peer review by experienced researchers in your field
- rapid publication on acceptance
- support for research data, including large and complex data types
- gold Open Access which fosters wider collaboration and increased citations
- maximum visibility for your research: over 100M website views per year

At BMC, research is always in progress.

Learn more [biomedcentral.com/submissions](https://www.biomedcentral.com/submissions)

